Lanthanide contraction effect on the alkaline hydrogen evolution and oxidation reactions activity in platinum–rare earth nanoalloys

Carlos Campos-Roldán, Raphaël Chattot, Frédéric Pailloux, Andrea Zitolo, Jacques Rozière, Deborah Jones, Sara Cavaliere

ARTICLE

Lanthanide Contraction Effect on the Alkaline Hydrogen Evolution and Oxidation Reactions Activity in Platinum-Rare Earth Nanoalloys

Received 00th January 20xx,
Accepted 00th January 20xx

DOI: 10.1039/x0xx00000x

Carlos A. Campos-Roldán,*[a] Raphaël Chattot,[a] Frédéric Pailloux,[b] Andrea Zitolo,[c] Jacques Roziere,[a] Deborah J. Jones,[a] and Sara Cavaliere*[a].

The hydrogen evolution/oxidation reactions (HER/HOR) play an important role in hydrogen energy conversion devices. Notwithstanding, the poor understanding of the sluggish HER/HOR kinetics on Pt in alkaline media is still a bottleneck. Herein, we have prepared a series of Pt-rare earth (RE) nanoalloys and, for the first time, systematically evaluated them towards the alkaline HER/HOR, and have identified the effect of the lanthanide contraction. *Operando* XAS measurements revealed that the induced compressive strain is not the sole kinetic descriptor, and that the chemical nature of the RE might modulate the adsorption and mobility of oxygenated-species, boosting the electrochemical reactions kinetics. This work provides insights on the property-activity trends of the unexplored Pt-RE/C nanoalloys in alkaline solution, and might inspire the rational design of electrocatalysts for the alkaline HER/HOR.

Introduction

The hydrogen economy represents a crucial component in achieving the current decarbonization targets.[1] Even though proton-exchange membrane (PEM) water electrolyzers and fuel cells (PEMWE and PEMFC, respectively) are the most efficient devices so far, technical and economic barriers still hamper their massive commercialization,[2] *e.g.*, electrocatalysts' high cost (use of expensive precious metals at high loadings), sluggish oxygen reactions kinetics, harsh corrosive environment, etc. In this context and due to the growing development of anion-exchange membranes (AEM),[3] water electrolyzers and fuel cells (AEMWE and AEMFC, respectively) have attracted attention due to their interesting advantages with respect to their PEM counterparts, namely, the possible use of more generally available non-precious metals, faster reaction kinetics for the oxygen reactions, relatively lower corrosion problems, *etc*. Notwithstanding, for still unclear reasons, the alkaline hydrogen evolution reaction (HER, cathodic reaction of an AEMWE) and the hydrogen oxidation reaction (HOR, anodic reaction of an AEMFC) on precious metal surfaces are at least two orders of magnitude slower than their acidic counterparts.[4] Therefore, the poor understanding of the sluggish alkaline HER/HOR kinetics on precious metal, especially on Pt-based surfaces, still limits the rational design of efficient electrocatalysts.

A widely use strategy to improve the activity of Pt-based electrocatalysts is by combining it (either by alloying or decorating its surface) with other metals, *e.g.*, Ru, Ni, Co, *etc*.[5] However, there is a wide debate in the literature concerning the role of the mixed metal on the electrocatalytic activity.[6-14] Although the compressive strain effect, induced by the alloying metal, is among the most studied properties in Pt-based electrocatalysts, its impact on the alkaline HER/HOR performance is still elusive, with studies that either support[12, 14] or refute[13] a positive effect.

On the other hand, research on Pt-rare earth (Pt-RE) nanoalloys as electrocatalysts has considerably increased in recent years.[15-23] Indeed, their key structural properties for electrocatalysis, such as the induced compressive strain, might be tuned by means of the lanthanide contraction.[24] Namely, the Pt-RE alloys can present an unusual $CaCu_5$-like hexagonal crystalline structure that accommodates the alloying elements of different atomic radius in a different way from face centred cubic (fcc) or hexagonal closed-package (hcp) alloys. While the lattice parameter *a* in the hexagonal structure continues its shortening through the lanthanide contraction, the *b* and *c* lattice parameters are considerably different due to the re-organization of the atoms. Thus, the lattice constant *a* will contract (shorter Pt-Pt distances) as the RE covalent radii decrease.[24] This trend is an interesting strategy to systematically investigate the effect of the induced strain in Pt-

[a] *ICGM, Univ. Montpellier, CNRS, ENSCM, 34095 Montpellier cedex 5, France.*
[b] *Institut P', CNRS - Université de Poitiers – ISAE-ENSMA - UPR 3346, 11 Boulevard Marie et Pierre Curie, Site du Futuroscope, TSA 41123, 86073 Poitiers cédex 9, France.*
[c] *Synchrotron SOLEIL, L'Orme des Merisiers, BP 48 Saint Aubin, 91192 Gif-sur-Yvette, France.*

†Electronic Supplementary Information (ESI) available: Complementary ICP-MS results, complementary TEM micrographs and particle size histograms, comparison between the acquired cyclic voltammograms at the RDE setup and the XAS electrochemical cell, the detailed explanation of the kinetic parameters determination, details of the HAADF-STEM/EELS, CO-stripping voltammograms and HER/HOR polarization curves. See DOI: 10.1039/x0xx00000x

based alloys. Moreover, Pt-RE nanoalloys have never been explored as alkaline HER/HOR electrocatalysts so far, and the high oxophilicity of the REs could also contribute to the bifunctional effect.[8, 9, 25]

Herein, we contribute to this field with new insights regarding the systematic study of the compressive strain in hexagonal Pt_5RE/C (RE= La, Ce or Nd) nanoalloys towards the alkaline HER/HOR. While the crystalline structure is maintained constant, the imposed compressive strain is modulated by the lanthanide contraction: as the atomic size of the RE steadily decreases (La > Ce > Nd), the imposed compressive strain increases (Pt_5La < Pt_5Ce < Pt_5Nd). This trend is confirmed using *operando* X-ray absorption spectroscopy (XAS) measurements, and the experimental alkaline HER/HOR activity is rationalized with the structural parameters derived from *operando* measurements.

Results and discussion

Pt_xRE/C (RE= La, Ce or Nd) nanoalloys were synthesized using the carbodiimide complex route proposed by Hu *et al.*[20] with some modifications, see experimental details in **Supplementary Information S1**. The XRD patterns shown in **Figure 1a** confirm the Pt-RE alloy formation, the crystalline structure of which comprises the hexagonal Pt_5RE arrangement (space group P6/mmm). The induced *ex situ* compressive strain shown in **Table S1** clearly shows the systematic effect of the lanthanide contraction in the structure of the nanoalloys, in agreement with Escudero-Escribano *et al.*[24] The Pt content in all samples, determined by ICP-MS, lies between 27-28 *% wt.*, giving a Pt:RE ratio of *ca.* 6:1 (see **Table S1**). TEM reveals the presence of nanoparticles (NPs) of *ca.* 6 nm and agglomerates of 12 nm dispersed over the carbon support (**Figure S1**). Furthermore, the HRTEM overview shown in **Figure 1b** resolves the atomic arrangement of the hexagonal Pt_5Nd (101) crystalline plane, revealing the lattice parameter a ~ 5 Å, in agreement with the XRD patterns.

As a representative example, combined HAADF-STEM/EELS analyses also attest to the presence of Pt and Ce in PtxCe/C (**Figure 1c**) and Pt and La in PtxLa/C (**Figure 1d**), which are consistent with a discernible Pt enrichment (< 1 nm) at the border of the NPs, in agreement with previous reports for PtxLa/C,[19] PtxCe/C[20, 21] and PtxNd/C.[26] The results presented above underpin that PtxLa/C, PtxCe/C and PtxNd/C electrocatalysts presents similar crystalline structure, chemical composition, local morphology and particle size, *c.f.* **Table S1**. Therefore, a proper comparison of the effect of the lanthanide contraction on the alkaline HER/HOR activity can be performed.

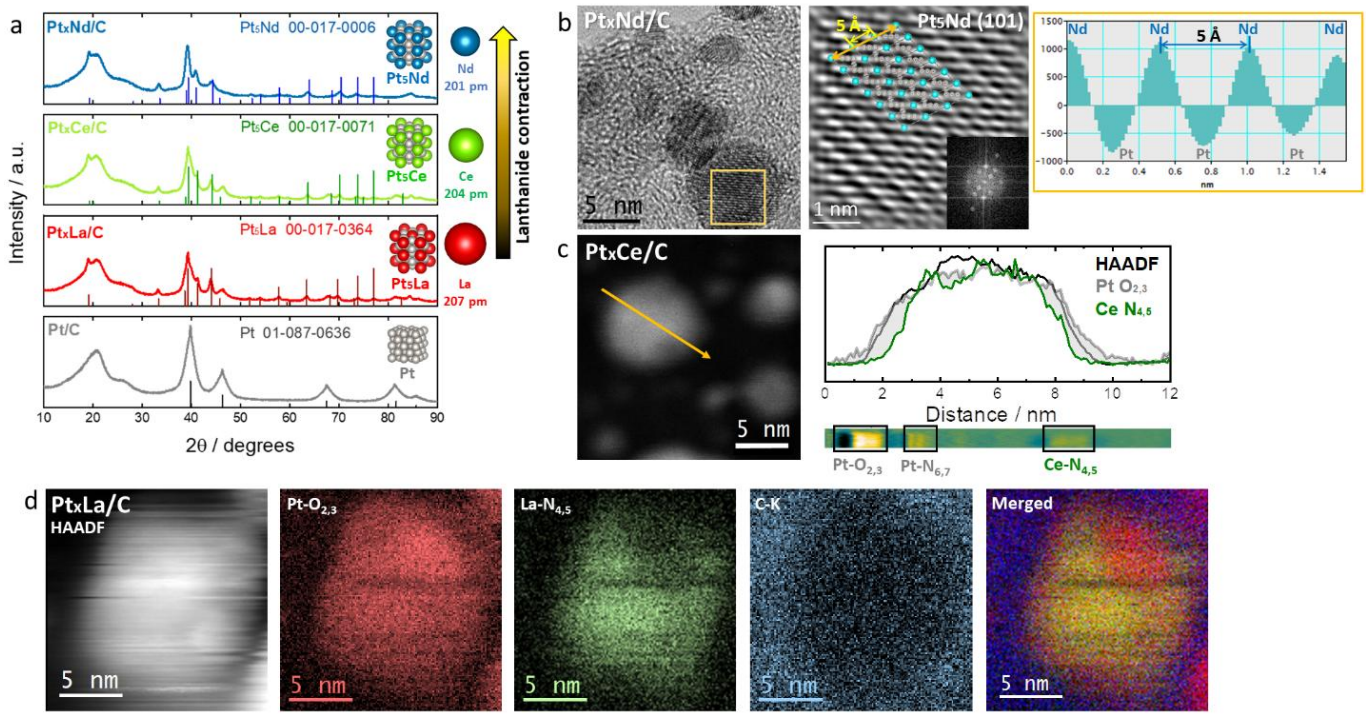

Fig. 1 (a) XRD patterns of PtxLa/C, PtxCe/C and PtxNd/C. Pt/C is used as reference. (b) Representative HRTEM micrographs of PtxNd/C (the insert corresponds to the power spectrum of the selected area); (c) representative HAADF-STEM/EELS analysis of (c) PtxCe/C (chemical line scan) and (d) PtxLa/C (chemical mapping).

ARTICLE

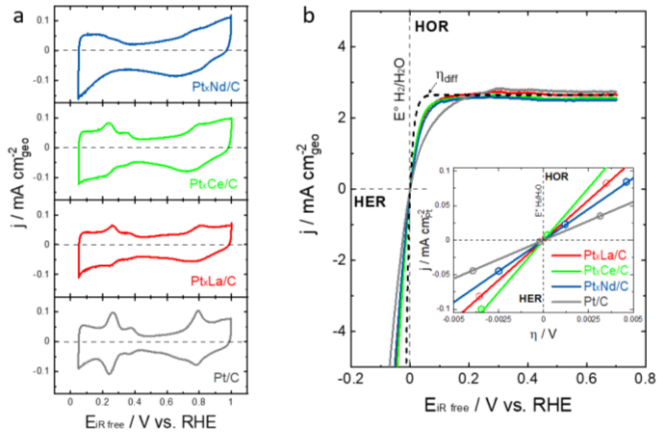

Fig. 2 (a) Cyclic voltammograms in N_2-saturated 0.1 M KOH at 20 mV s^{-1}, and (b) HER/HOR polarization curves in H_2-saturated 0.1 M KOH at 10 mV s^{-1} at 1600 rpm of PtxLa/C, PtxCe/C and PtxNd/C. The black dashed line represents the Nernstian diffusion overpotential (η_{diff}) curve. Measurements were carried out at 26 ±1 °C. Pt/C is used as reference.

Figure 2 shows the results extracted from RDE measurements in 0.1 M KOH. The cyclic voltammogram of the Pt/C reference in **Figure 2a** depicts the well-known features of Pt polycrystalline NPs in alkaline medium on a glass-free setup.[27] However, the acquired signals in the profiles of the Pt-RE/C electrocatalysts differ from those of the reference, suggesting the existence of modifications in their surface electrochemistry. By overlapping the cyclic voltammograms (**Supplementary Information S3**), the position of the H_{upd} peaks of PtxLa/C and PtxCe/C are negatively shifted with respect to Pt/C. In the case of PtxNd/C, the H_{upd} peaks are not clearly resolved. This feature might be related, to a certain extent (see discussion below), to the weakening of the Pt-H bond strength derived from the *d*-band shifting caused by the alloying effect. Indeed, similar shifts in the H_{upd} region have been observed in sputter-clean bulk polycrystalline Pt-RE electrodes in acid medium.[24]

The HER/HOR polarization curves, **Figure 2b**, reveal that Pt-RE/C electrocatalysts present enhanced intrinsic activity with respect to the Pt/C reference, and a shift towards the Nernstian diffusion overpotential curve is observed.[28] This observation is also reflected in the micropolarization region (insert in **Figure 2b**) and in the turnover frequency values (TOF), defined as the number of H_2 molecules evolved (HER) or consumed (HOR) per active site per unit time[29] (**Table 1**), where an activity enhancement trend PtxCe/C > PtxLa/C > PtxNd/C > Pt/C is observed. The mass activity values (I_m) also indicate an enhancement factor using the Pt-RE/C nanoalloys, with respect to the Pt/C reference, of *ca.* 2.8, 2.0 and 1.6 for PtxCe/C, PtxLa/C and PtxNd/C, respectively.

To determine the local structure of the Pt-RE/C nanoalloys under electrochemical conditions, *operando* XAS measurements were performed. It is important to note that the surface electrochemistry acquired in the electrochemical cell for the *operando* XAS measurements match satisfactorily with the profiles obtained using the RDE setup (**Supplementary Information S5**), allowing comparison and evaluation of the structural properties under the electrochemical conditions.

The *operando* Pt L_3 edge X-ray absorption near-edge structure (XANES) spectra acquired at 0.1 V_{RHE}, shown in **Figure 3a**, reveal an increased white line intensity for the Pt-RE electrocatalysts (PtxCe/C > PtxLa/C > PtxNd/C ≥ Pt/C). The white line intensity is directly related to the Pt 5*d* band occupancy:[30] the higher the white line intensity, the higher the unoccupied valence states, suggesting a higher oxidation degree as the white line intensity increases. This result suggests that, at 0.1 V_{RHE}, PtxCe/C and PtxLa/C might present higher oxygenated-species adsorption (OH_{ads} and/or $H_2O{\downarrow}_{ads}$) than PtxNd/C and Pt/C. Jia *et al.*[8] have also observed a relationship between the increased white line intensity and enhanced HER/HOR activity with Pt-Ru systems. The effect of this feature on the HER/HOR kinetics will be discussed below.

Moreover, the results of the fitting of the filtered Fourier transformed *operando* extended X-ray absorption fine structure (EXAFS) spectra, *cf.* **Figure 3b and Table 2**, clearly indicate that the nearest neighbour Pt-Pt interatomic distances (d_{Pt-Pt}) in the Pt-RE/C nanoalloys are shorter than in the Pt/C reference. Indeed, the d_{Pt-Pt} contraction relative to Pt/C follows the trend PtxLa/C (-0.87%) > PtxCe/C (-1.34%) > PtxNd/C (-1.78%), and reflects the effect of the lanthanide contraction under the electrochemical conditions: as the atomic size of the RE through the lanthanide series steadily decreases (La > Ce > Nd), the d_{Pt-Pt} are shorter and, therefore, the imposed compressive strain increases.[24]

Table 1. Kinetic parameters extracted from the RDE characterization of PtxLa/C, PtxCe/C and PtxNd/C. Pt/C is used as reference. TOF and I_m values are calculated at η= -10mV for the HER and η= 10mV for the HOR. Details for the calculation are given in the **Supplementary Information S4**.

Sample	ECSA ($m^2\ g_{Pt}^{-1}$)	j_0 ($mA\ cm^{-2}_{Pt}$)	Rct_0 ($\Omega\ cm^2_{Pt}$)	$TOF_{@\eta=-10\ mV}$ ($\#H_2\ site^{-1}\ s^{-1}$)	$TOF_{@\ \eta=10\ mV}$ ($\#H_2\ site^{-1}\ s^{-1}$)	$I_{m@\ \eta=-10\ mV}$ ($A\ mg^{-1}_{Pt}$)	$I_{m@\ \eta=10\ mV}$ ($A\ mg^{-1}_{Pt}$)
Pt/C	55.5 ±2.1	0.46 ±0.01	56.28 ±1.73	12.63 ±0.66	12.21 ±0.92	0.057 ±0.003	0.055 ±0.004
Pt_xLa/C	47.6 ±3.6	0.61 ±0.04	42.43 ±3.00	26.14 ±2.95	27.76 ±1.96	0.104 ±0.011	0.111 ±0.007
Pt_xCe/C	47.0 ±3.4	0.80 ±0.04	32.99 ±2.46	34.23 ±2.04	38.55 ±2.60	0.135 ±0.008	0.152 ±0.010
Pt_xNd/C	48.2 ±2.5	0.55 ±0.03	46.80 ±2.43	21.52 ±2.34	23.03 ±2.64	0.087 ±0.009	0.093 ±0.010

Rationalizing the $TOF_{@\ \eta=10\ mV}$ values reported in **Table 1** and the local structural properties under the electrochemical conditions shown in **Table 2**, a volcano-like curve emerged, **Figure 4**, suggesting a maximum TOF value for PtxCe/C, achieving a compressive strain of -1.34 %.

For the sake of clarity, we will discuss these interesting experimental trends with the current mechanistic understanding of the alkaline HER/HOR. Although the controversy in the literature, it is accepted that the alkaline HER/HOR on Pt surfaces follows the Volmer-Tafel/Tafel-Volmer mechanism, the reaction determining step being the Volmer step[31]:

Volmer step: $H_2O + * + e^- \rightleftharpoons * - H_{ads} + OH^-$

Tafel step: $2 * - H_{ads} \rightleftharpoons H_2$

Where * states an active site on the surface.

Following classical *d*-band theory, weakening the strength of the hydrogen binding energy (HBE) through the compressive strain effect improves the Volmer step through a Brønsted-Evans-Polanyi (BEP) relationship.[32] Although this argument is particularly true in acidic electrolytes, recent contributions have suggested important deviations of the BEP relationship at high pH values,[31] concluding that other complex phenomena modulate the electrochemical kinetics in alkaline medium.

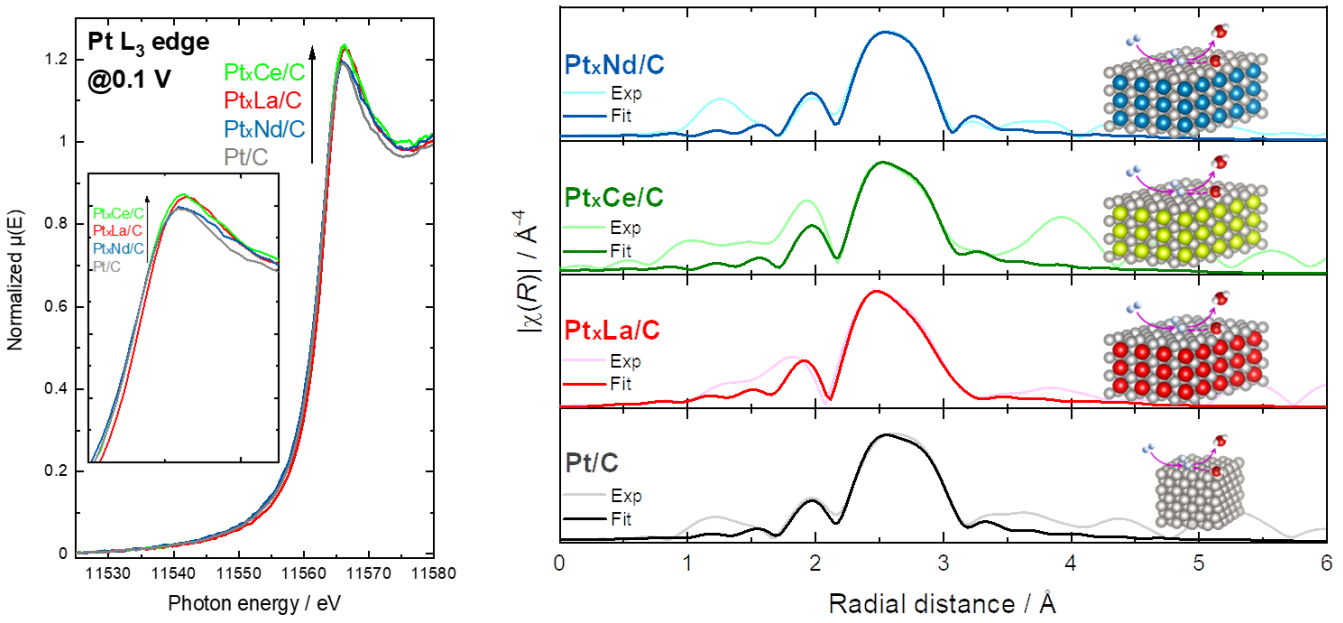

Fig. 3 *Operando* Pt L_3-edge (a) XANES spectra, and (b) EXAFS spectra and the corresponding best fits of PtxLa/C, PtxCe/C and PtxNd/C. Measurements were carried out in H_2-saturated 0.1 M KOH at 0.1 V_{RHE}. Pt/C is used as reference.

Table 2. Best first-shell fit parameters obtained from the Pt L_3-edge EXAFS analysis acquired at 0.1 V_{RHE} of PtxLa/C, PtxCe/C and PtxNd/C. Pt/C is used as reference. The amplitude reduction factor S_0^2 was set at 0.8.

	Path	N	R (Å)	*ε (%)	σ^2	ΔE	R factor
Pt/C	Pt – Pt	9.7 ±1.0	2.749 ±0.005	0	0.0049 ±0.0006	6.87 ±0.85	0.014
Pt_xLa/C	Pt – Pt	5.5 ±0.3	2.725 ±0.007	-0.87	0.0052 ±0.0009	5.48 ±1.06	0.020
	Pt – La	0.4 ±0.2	3.155 ±0.007	--	0.0039 ±0.0011	9.14 ±0.55	
Pt_xCe/C	Pt – Pt	6.4 ±1.0	2.712 ±0.006	-1.34	0.0045 ±0.0009	5.45 ±1.49	0.024
	Pt – Ce	0.5 ±0.2	3.097 ±0.080	--	0.0059 ±0.0010	9.92 ±0.95	
Pt_xNd/C	Pt – Pt	6.3 ±0.2	2.700 ±0.006	-1.78	0.0052 ±0.0004	7.46 ±0.65	0.012
	Pt – Nd	0.5 ±0.2	3.167 ±0.080	--	0.0097 ±0.0006	6.64 ±1.85	

*Relative to Pt/C at 0.1 V_{RHE}.

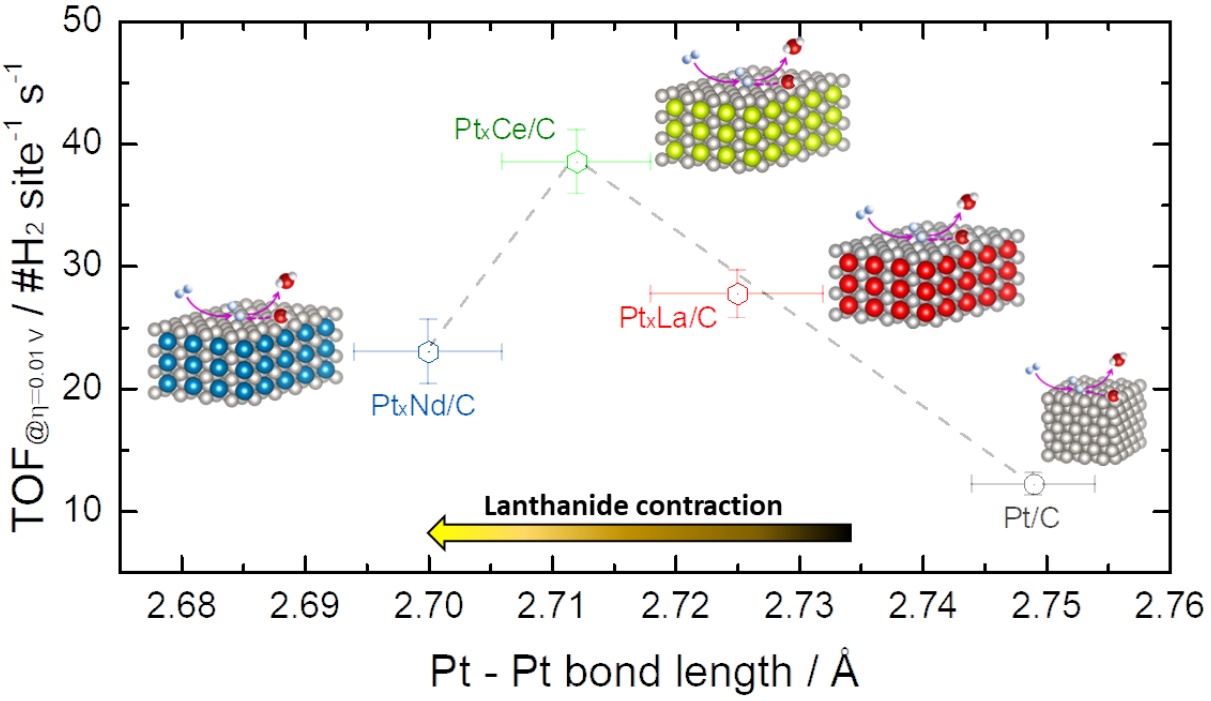

Fig. 4 Relationship between the Pt-Pt bond length and the TOF (measured at η= 10 mV), of PtxLa/C, PtxCe/C and PtxNd/C. Pt/C is used as reference.

Even though straightforward relationships between the induced compressive strain and the weakening of the HBE has been used as the sole kinetic descriptor for Pt-based nanoalloys towards the alkaline HER/HOR,[12, 14] **Figure 4** reveals that the alkaline HER/HOR activity of the present Pt_xRE/C nanoalloys reaches a critical value as the induced compressive strain increases. Therefore, the compressive strain might not explain completely the observed activity enhancement, in agreement with the previous work on PtCu/C.[13]

On the other hand, it has been proposed that the origin of the H_{upd} peaks of Pt surfaces in alkaline electrolytes stem from the exchange between H_{ads} and OH_{ads}[31] or a specifically H_2O_{ads} with the oxygen facing towards the electrode ($H_2O{\downarrow}_{ads}$)[33]. Therefore, H_{ads} might not be the only surface species present during the alkaline HER/HOR, suggesting a competition between H_{ads} and oxygen adsorbates (OH_{ads} and $H_2O{\downarrow}_{ads}$)[31]: the electrochemical kinetics might be governed by the activation barriers and thermodynamics connecting each elementary step in the reaction mechanism, *i.e.,* H_{ads}, OH_{ad} and H_2O_{ads}. In this sense, it has been reported that the hydroxide binding energy (OHBE)[7] or the interfacial water structure[33, 34] should be strengthened to boost the alkaline HER/HOR. Looking at **Figure 3a**, the increased white line intensity of Pt_xCe/C indicates a higher oxidation state relative to Pt/C, suggesting an enhanced primary desorption of H_{ads} in this potential region,[8] in line with the negative shift of the H_{upd} peaks shown in **Supplementary Information S3.** Indeed, the interaction between OH^- and Pt-based surfaces, in alkaline medium, can be monitored using carbon monoxide as a molecular probe,[9] since the alkaline CO electro-oxidation process on Pt-based surfaces proceeds through a Langmuir-Hinshelwood reaction between the adsorbed states of CO and OH_{ads}[35]:

$$CO_{ads} + OH_{ads} + OH^- \rightarrow CO_2 + e^- + H_2O$$

Figure S6 shows the CO-stripping voltammograms of the Pt-RE/C series, along with the Pt/C benchmark. From **Figure S6**, a main CO electro-oxidation peak shift is observed towards lower electrode potential for the Pt-RE/C nanoalloys relative to the Pt/C reference. This feature might suggest a higher supply of reactive OH^- species to remove the adsorbed CO from the surface of the Pt-RE nanoalloys. Nevertheless, the electronic modification caused by the compressive strain might also weaken the Pt-CO bond energy.[36]

This promoting effect might facilitate the Volmer step *via* the bifunctional mechanism[8, 9, 25] or by facilitating the mobility of charged intermediates through the double layer.[33, 34] Considering that the basic strength of lanthanides decreases as the RE size decreases, it is plausible that the chemical nature of the RE plays an important role for the oxygenated-species adsorption and mobility during the alkaline HER/HOR.

It should be noted, however, that the Volmer step inevitably disrupts the interfacial water structure, and thus water reorganization energy should be considered. Therefore, an ideal HER/HOR electrocatalyst should balance the HBE and the interaction with oxygen-based intermediates (OHBE or water reorganization energy) to facilitate, respectively, the Tafel and Volmer steps. Further DFT calculations might provide fundamental insights on the effect of the lanthanide contraction on the water reorganization energy.

Conclusions

In conclusion, a series of Pt-RE/C (RE= La, Ce or Nd) nanoalloys were prepared and, for the first time, evaluated as electrocatalysts for the alkaline HER/HOR. The hexagonal Pt_5RE crystalline structure, chemical composition, local morphology and particle size were kept similar, allowing for systematic examination of the lanthanide contraction effect on the electrocatalytic activity towards the alkaline HER/HOR. *Operando* XAS measurements revealed that the compressive strain is not the sole kinetic descriptor for the alkaline HER/HOR, with the maximum activity being observed with Pt_xCe/C (ε = -1.34 %). Interestingly, our results also suggest that the chemical nature of the RE might modulate the adsorption of oxygenated-species, *i.e.*, OH_{ads} and/or $H_2O{\downarrow}_{ads}$, and boosts the electrochemical kinetics.

This work provides insights on the property-activity trends of the unexplored Pt-RE/C nanoalloys and might inspire the rational design of electrocatalysts for the alkaline HER/HOR.

Conflicts of interest

There are no conflicts to declare.

Acknowledgements

R.C received financial support from the French National Research Agency through the HOLYCAT project (grant number n◦ ANR-22-CE05-0007). We gratefully acknowledge Synchrotron SOLEIL (Gif-sur Yvette, France) for provision of synchrotron radiation facilities at beamline SAMBA under the proposal number 20211337.

References

1. I. Staffell, D. Scamman, A. Velazquez Abad, P. Balcombe, P. E. Dodds, P. Ekins, N. Shah and K. R. Ward, *Energy & Environmental Science*, 2019, **12**, 463-491.
2. R. L. Borup, A. Kusoglu, K. C. Neyerlin, R. Mukundan, R. K. Ahluwalia, D. A. Cullen, K. L. More, A. Z. Weber and D. J. Myers, *Current Opinion in Electrochemistry*, 2020, **21**, 192-200.
3. Y. Yang, P. Li, X. Zheng, W. Sun, S. X. Dou, T. Ma and H. Pan, *Chem Soc Rev*, 2022, **51**, 9620-9693.
4. J. Durst, A. Siebel, C. Simon, F. Hasché, J. Herranz and H. A. Gasteiger, *Energy Environ. Sci.*, 2014, **7**, 2255-2260.
5. C. A. Campos-Roldán and N. Alonso-Vante, *Electrochemical Energy Reviews*, 2019, **2**, 312-331.
6. Y. H. Wang, X. T. Wang, H. Ze, X. G. Zhang, P. M. Radjenovic, Y. J. Zhang, J. C. Dong, Z. Q. Tian and J. F. Li, *Angew Chem Int Ed Engl*, 2021, **60**, 5708-5711.
7. I. T. McCrum and M. T. M. Koper, *Nature Energy*, 2020, **5**, 891-899.
8. J. Li, S. Ghoshal, M. K. Bates, T. E. Miller, V. Davies, E. Stavitski, K. Attenkofer, S. Mukerjee, Z. F. Ma and Q. Jia, *Angew Chem Int Ed Engl*, 2017, **56**, 15594-15598.
9. C. A. Campos-Roldán and N. Alonso-Vante, *Journal of Solid State Electrochemistry*, 2021, **25**, 187-194.
10. F. J. Sarabia, P. Sebastian-Pascual, M. T. M. Koper, V. Climent and J. M. Feliu, *ACS Appl Mater Interfaces*, 2019, **11**, 613-623.
11. Q. Zhang, K. Kusada, D. Wu, T. Yamamoto, T. Toriyama, S. Matsumura, S. Kawaguchi, Y. Kubota and H. Kitagawa, *J Am Chem Soc*, 2022, **144**, 4224-4232.
12. X. Wang, Y. Zhu, A. Vasileff, Y. Jiao, S. Chen, L. Song, B. Zheng, Y. Zheng and S.-Z. Qiao, *ACS Energy Letters*, 2018, **3**, 1198-1204.
13. L. Jiao, E. Liu, S. Hwang, S. Mukerjee and Q. Jia, *ACS Catalysis*, 2021, **11**, 8165-8173.
14. T. Gong, H. Alghamdi, D. Raciti and A. S. Hall, *ACS Energy Letters*, 2022, **8**, 685-690.
15. C. A. Campos-Roldán, D. J. Jones, J. Rozière and S. Cavaliere, *ChemCatChem*, 2022, **14**, e202200334.
16. C. A. Campos-Roldán, A. Parnière, N. Donzel, F. Pailloux, P.-Y. Blanchard, D. J. Jones, J. Rozière and S. Cavaliere, *ACS Applied Energy Materials*, 2022, **5**, 3319-3328.
17. C. A. Campos-Roldán, F. Pailloux, P.-Y. Blanchard, D. J. Jones, J. Rozière and S. Cavaliere, *ACS Catal.*, 2021, **11**, 13519-13529.
18. C. A. Campos-Roldan, F. Pailloux, P. Y. Blanchard, D. J. Jones, J. Roziere and S. Cavaliere, *Nanoscale Adv*, 2021, **4**, 26-29.
19. T. Gunji, S. Tanaka, T. Inagawa, K. Otsuka and F. Matsumoto, *ACS Appl. Nano Mater.*, 2022, **5**, 4958-4965.
20. Y. Hu, J. O. Jensen, L. N. Cleemann, B. A. Brandes and Q. Li, *J Am Chem Soc*, 2020, **142**, 953-961.
21. H. Itahara, Y. Takatani, N. Takahashi, S. Kosaka, A. Nagoya, M. Inaba, Y. Kamitaka and Y. Morimoto, *Chem. Mater.*, 2021, **34**, 422-429.
22. S.-L. Xu, S. Zhao, W.-J. Zeng, S. Li, M. Zuo, Y. Lin, S. Chu, P. Chen, J. Liu and H.-W. Liang, *Chemistry of Materials*, 2022, **34**, 10789-10797.
23. Q. Zhou, J. O. Jensen, L. N. Cleemann, Q.-F. Li and Y. Hu, *Advanced Sensor and Energy Materials*, 2022, **1**, 100025-100033.
24. M. Escudero-Escribano, P. Malacrida, M. Hansen, U. Vej-Hansen, A. Velázquez-Palenzuela, V. Tripkovic, J. Schiøtz,

J. Rossmeisl, I. Stephens and I. Chorkendorff, *Science*, 2016, **352**, 73-76.
25. D. Strmcnik, M. Uchimura, C. Wang, R. Subbaraman, N. Danilovic, D. van der Vliet, A. P. Paulikas, V. R. Stamenkovic and N. M. Markovic, *Nature Chemistry*, 2013, **5**, 300-306.
26. C. A. Campos-Roldán, R. Chattot, J.-S. Filhol, H. Guesmi, F. Pailloux, R. Bacabe, P.-Y. Blanchard, A. Zitolo, J. Drnec, D. J. Jones and S. Cavaliere, *ACS Catalysis*, 2023, **13**, 7417-7427.
27. C. A. Campos-Roldán, R. G. González-Huerta and N. Alonso-Vante, *Journal of The Electrochemical Society*, 2018, **165**, J3001-J3007.
28. H. A. G. W. Sheng, Y. Shao-Horn, *Journal of The Electrochemical Society*, 2010, **157**, B1529-B1536.
29. J. Hansen, Prats, H., Toudahl, K., Secher, M., Chan, K., Kibsgaard, J., Chorkendorff, I., *ACS Energy Lett.*, 2021, **6**, 1175−1180.
30. J. Timoshenko and B. Roldan Cuenya, *Chem Rev*, 2021, **121**, 882-961.
31. L. Rebollar, S. Intikhab, N. J. Oliveira, Y. Yan, B. Xu, I. T. McCrum, J. D. Snyder and M. H. Tang, *ACS Catalysis*, 2020, **10**, 14747-14762.
32. W. Sheng, Z. Zhuang, M. Gao, J. Zheng, J. G. Chen and Y. Yan, *Nat Commun*, 2015, **6**, 5848.
33. E. Liu, L. Jiao, J. Li, T. Stracensky, Q. Sun, S. Mukerjee and Q. Jia, *Energy & Environmental Science*, 2020, **13**, 3064-3074.
34. I. Ledezma-Yanez, W. D. Z. Wallace, P. Sebastián-Pascual, V. Climent, J. M. Feliu and M. T. M. Koper, *Nature Energy*, 2017, **2**.
35. T. J. Schmidt, P. N. Ross and N. M. Markovic, *The Journal of Physical Chemistry B*, 2001, **105**, 12082-12086.
36. J. Ma, A. Habrioux, Y. Luo, G. Ramos-Sanchez, L. Calvillo, G. Granozzi, P. B. Balbuena and N. Alonso-Vante, *Journal of Materials Chemistry A*, 2015, **3**, 11891-11904.